Physica D 468 (2024) 134302

Contents lists available at ScienceDirect

Physica D

journal homepage: www.elsevier.com/locate/physd

The dynamics around the collinear points of the elliptic three-body problem: A normal form approach

Alessandra Celletti, Christoph Lhotka *, Giuseppe Pucacco

Department of Mathematics, University of Roma Tor Vergata, Via della Ricerca Scientifica 1, 00133 Roma, Italy

ARTICLE INFO

Communicated by Victor M. Perez-Garcia

Keywords:
Elliptic three-body problem
Lagrangian points
Collinear points
Halo orbits
Lissajous orbits

ABSTRACT

We study the dynamics of the collinear points in the planar, restricted three-body problem, assuming that the primaries move on an elliptic orbit around a common barycenter. The equations of motion can be conveniently written in a rotating–pulsating barycentric frame, taking the true anomaly as independent variable. We consider the Hamiltonian modeling this problem in the extended phase space and we implement a normal form to make a center manifold reduction. The normal form provides an approximate solution for the Cartesian coordinates, which allows us to construct several kinds of orbits, most notably planar and vertical Lyapunov orbits, and halo orbits. We compare the analytical results with a numerical simulation, which requires special care in the selection of the initial conditions.

1. Introduction

Despite their instability, the collinear equilibrium points of the planar, circular, restricted three-body problem (hereafter, PCR3BP) play a key role in Celestial Mechanics and Astrodynamics. In the PCR3BP, a small particle moves in the gravitational field of two primaries, which orbit around each other on a circular orbit; moreover, all bodies move in the same plane. The collinear points, which are equilibria in the synodic reference frame, have been used to design space trajectories [1,2] and they are considered privileged positions where to place spacecraft or instruments. There are many works devoted to analytical and numerical solutions around the collinear points in the circular problem (see, e.g., [3–7]). In this work, we extend the study of the dynamics around the collinear points assuming that the primaries move on an elliptic orbit, thus providing a more *realistic* description.

An analytical approach based on the construction of a resonant normal form has been applied in [6,7] in the case of the spatial *circular* problem. This approach provides an integrable 3-DOF Hamiltonian which captures both the hyperbolic dynamics normal to the center manifold and the elliptic dynamics on it. This analytical approach allows us also to compute approximate solutions for periodic and quasi-periodic orbits, including those associated to 1:1 resonant bifurcations. We remark that the method can be easily generalized to include perturbing effects like the Solar radiation pressure and the oblateness of the primaries [8,9].

In this work, we extend the construction of the analytical solution to the elliptic case by computing a suitable normal form, which describes Lyapunov planar orbits, Lyapunov vertical orbits, halo orbits; these orbits are characterized by prescriptions on the normal modes or by resonant conditions. As it is well known [10–12], in the planar, elliptic, restricted three-body problem, it is convenient to introduce a rotating–pulsating frame, which rotates with the true anomaly of the elliptic orbit, which is taken as independent variable; moreover, the coordinates are rescaled with the orbital radius. The Hamiltonian describing this problem depends on the true anomaly and therefore it is useful to consider it in the extended phase space by adding a dummy action conjugated to the true anomaly, thus obtaining a 4DOF Hamiltonian. In practice, however, the normal-form dynamics retains all the properties of the circular case and it is effectively an integrable 3-DOF problem. The time dependence is encoded in the generating function of the normalizing transformation and becomes apparent when the solutions are mapped back to the original variables.

We provide the explicit expressions of the normal form Hamiltonian for the collinear points L_1, L_2 and we give examples of the main families of periodic orbits for several cases of interest in astrodynamical applications. We remark that, in the work [13], the same problem has been treated with the Poincaré–Lindstedt method. The normal-form construction and the solutions thereof reproduces the results in [13] with additional dynamical clues. A first order resonant normal form already allows us to analytically compute the bifurcation threshold of the halo family which, for L_1 and L_2, turns out to be slightly higher than in the corresponding (namely, same mass ratio μ) circular problem.

In the specific case of the Earth–Moon system some Lyapunov and halo orbits are given together with some examples of isolated periodic

* Corresponding author.
E-mail addresses: celletti@mat.uniroma2.it (A. Celletti), lhotka@mat.uniroma2.it (C. Lhotka), pucacco@roma2.infn.it (G. Pucacco).

https://doi.org/10.1016/j.physd.2024.134302
Received 19 March 2024; Received in revised form 16 July 2024; Accepted 17 July 2024
Available online 23 July 2024

orbits with higher commensurability [14,15]. Explicit expressions of the generating functions of the Lie transform are given in order to compute invariant manifolds (periodic orbits and invariant tori) at second order in the expansion.

The results are validated by a numerical integration of the equations of motion in which the initial conditions are given by the normal form procedure and carefully refined in order to find the given orbit, either Lyapunov or halo orbit. Finally, we mention that to get reliable trajectories, it is essential to use the symmetry of the periodic orbit which leads to some constraints in the initial conditions.

The paper is organized as follows. In Section 2 we give the setup in the elliptic case and we proceed with the center manifold reduction; in Section 3 we describe the resonant normal form; in Section 4 the normal form is used to compute the bifurcation thresholds of the halo orbits; Section 5 provides examples of different orbits for the L_1 equilibrium point in the Earth–Moon case; Section 6 presents numerical simulations with a dedicated procedure to refine the initial conditions.

2. Collinear points and center manifold reduction

In this Section, we present the Hamiltonian of the elliptic, restricted three-body problem in the rotating–pulsating frame (Section 2.1), we discuss the location of the collinear points (Section 2.2), we introduce the Hamiltonian in the extended phase space (Section 2.3), we compute the quadratic part of the Hamiltonian in suitable coordinates (Section 2.4) and we briefly recall the main results of the center manifold reduction (Section 2.5).

2.1. The rotating–pulsating Hamiltonian

We consider a satellite S orbiting in the gravitational field of two primaries, P_1 and P_2 with masses, respectively, m_1 and m_2 (with $m_2 \le m_1$). We assume that the primaries orbit around their common barycenter on a Keplerian ellipse with semimajor axis a and eccentricity e. Denoting by h the angular momentum constant, related to the orbital elements by

$$h^2 = a(1-\mathrm{e}^2)\ ,$$

the orbital radius r is given by

$$r(f) = \frac{h^2}{1+\mathrm{e}\cos f}\ , \tag{2.1}$$

where f is the true anomaly.

We consider a *rotating–pulsating* barycentric frame, say (O,X,Y,Z), which is obtained as in [11] (see also [12]) starting from a set of coordinates in a fixed frame with origin coinciding with the barycenter O of the primaries, transforming the coordinates to a frame rotating with the true anomaly of the elliptic orbit (rotating frame), then rescaling the coordinates by the radius r (pulsating frame) and taking the true anomaly, instead of time, as independent variable. The latter choice implies that the time derivative is transformed into

$$\frac{d}{dt} = \frac{df}{dt}\frac{d}{df} = \frac{h}{r(f)^2}\frac{d}{df} = \frac{(1+\mathrm{e}\cos f)^2}{h^3}\frac{d}{df}\ ;$$

in the following, we will denote by a prime the derivative with respect to the true anomaly.

In the non-uniformly rotating–pulsating frame (O,X,Y,Z), the equations of motion of the satellite are given by (see [11], Section 10.3.2.3):

$$\begin{aligned} X'' - 2Y' &= \frac{\partial\Omega}{\partial X} \\ Y'' + 2X' &= \frac{\partial\Omega}{\partial Y} \\ Z'' + Z &= \frac{\partial\Omega}{\partial Z}\ , \end{aligned} \tag{2.2}$$

where the *potential* has the form

$$\Omega(X,Y,Z,f) = \frac{1}{1+\mathrm{e}\cos f}\left[\frac{1}{2}(X^2+Y^2+Z^2) + \frac{1-\mu}{r_1} + \frac{\mu}{r_2} + \frac{1}{2}\mu(1-\mu)\right] \tag{2.3}$$

with

$$\mu = \frac{m_2}{m_1+m_2}$$

and where the distances r_1, r_2 from the primaries, which are located at $(\mu,0,0)$, $(-1+\mu,0,0)$, are given by

$$r_1 = [(X-\mu)^2+Y^2+Z^2]^{\frac{1}{2}}\ , \qquad r_2 = [(X+1-\mu)^2+Y^2+Z^2]^{\frac{1}{2}}\ .$$

Denoting by p_X, p_Y, p_Z the momenta conjugated to X, Y, Z, the equations (2.2) are associated to the 3D non-autonomous Hamiltonian function

$$\begin{aligned} H(p_X,p_Y,p_Z,X,Y,Z,f) =& \frac{1}{2}(p_X^2+p_Y^2+p_Z^2) + Yp_X - Xp_Y \\ &+ \frac{1}{2}(X^2+Y^2+Z^2) - \Omega(X,Y,Z,f)\ . \end{aligned} \tag{2.4}$$

We consider such Hamiltonian on the collisionless manifold $\mathcal{P}_c \subset \mathbb{R}^3 \times \mathbb{R}^3$, defined as

$$\mathcal{P}_c \equiv \{(p_X,p_Y,p_Z),(X,Y,Z) \in \mathbb{R}^3\times\mathbb{R}^3 :\ r_1(X,Y,Z)\neq 0,\ r_2(X,Y,Z)\neq 0\}$$

and we endow $\mathcal{P}_c$ with the standard symplectic form

$$\omega_s = dp_X \wedge dX + dp_Y \wedge dY + dp_Z \wedge dZ\ .$$

2.2. The collinear points

We denote by L_1, L_2, L_3 the collinear equilibrium points inheriting the notation of the circular case. We underline that the reference frames are oriented in such a way that L_2 lies at the left of the smaller primary, while L_3 is at the right of the larger primary.

Let γ_j, $j=1,2,3$, be the distances of the collinear equilibrium points from the closest primary. The collinear equilibrium positions are the solutions of the equations

$$\frac{\partial\Omega}{\partial X} = 0\ , \qquad \frac{\partial\Omega}{\partial Y} = 0\ , \qquad \frac{\partial\Omega}{\partial Z} = 0$$

with the condition $Y=Z=0$. It can be shown (see, e.g., [12]) that the γ_j's are the solutions of the following 5th order Euler's equations:

$$\begin{aligned} \gamma_1^5 - (3-\mu)\gamma_1^4 + (3-2\mu)\gamma_1^3 - \mu\gamma_1^2 + 2\mu\gamma_1 - \mu = 0 \qquad &\text{for} \quad L_1 \\ \gamma_2^5 + (3-\mu)\gamma_2^4 + (3-2\mu)\gamma_2^3 - \mu\gamma_2^2 - 2\mu\gamma_2 - \mu = 0 \qquad &\text{for} \quad L_2 \\ \gamma_3^5 + (2+\mu)\gamma_3^4 + (1+2\mu)\gamma_3^3 - (1-\mu)\gamma_3^2 - 2(1-\mu)\gamma_3 - (1-\mu) = 0 \qquad &\text{for} \quad L_3\ . \end{aligned}$$

As in the circular problem, for each L_k, $k=1,2,3$, we translate the origin so that it coincides with a collinear point: we introduce new coordinates (x,y,z) through the following transformation

$$X = \mp\gamma_j x + \mu + a_j\ , \qquad Y = \mp\gamma_j y\ , \qquad Z = \gamma_j z\ . \tag{2.5}$$

The transformation (2.5) is used to simplify the new Hamiltonian through a rescaling translation. In (2.5), the upper signs hold for L_1, L_2, while the lower signs hold for L_3 and $a_1 = -1+\gamma_1$, $a_2 = -1-\gamma_2$, $a_3 = \gamma_3$. In this way, the collinear 'equilibria' in the elliptic problem, are actually pulsating with the rotating frame.

We introduce the energy as the value of the Hamiltonian computed at the initial conditions; this quantity is a function of the true anomaly. The relation between the energy E in rotating–pulsating synodic coordinates and the energy $\widetilde{\mathcal{E}}$ in the local coordinates, in virtue of the rescaling, is given by

$$\begin{aligned} L_1 :\ E &= \widetilde{\mathcal{E}}\gamma_1^2 - \frac{1}{2}(1-\gamma_1-\mu)^2 - \frac{\mu}{\gamma_1} - \frac{1-\mu}{1-\gamma_1} \\ L_2 :\ E &= \widetilde{\mathcal{E}}\gamma_2^2 - \frac{1}{2}(1+\gamma_2-\mu)^2 - \frac{\mu}{\gamma_2} - \frac{1-\mu}{1+\gamma_2} \\ L_3 :\ E &= \widetilde{\mathcal{E}}\gamma_3^2 - \frac{1}{2}(\gamma_3+\mu)^2 - \frac{1-\mu}{\gamma_3} - \frac{\mu}{1+\gamma_3}\ . \end{aligned}$$

Introducing the coefficients $c_n(\mu)$, $n \ge 2$, given by

$$c_n(\mu) = \frac{1}{\gamma_1^3}\left(\mu + (-1)^n\frac{(1-\mu)\gamma_1^{n+1}}{(1-\gamma_1)^{n+1}}\right) \qquad \text{for} \quad L_1$$

$$c_n(\mu) = \frac{(-1)^n}{\gamma_2^3}\left(\mu + \frac{(1-\mu)\gamma_2^{n+1}}{(1+\gamma_2)^{n+1}}\right) \qquad \text{for} \quad L_2$$
$$c_n(\mu) = \frac{(-1)^n}{\gamma_3^3}\left(1-\mu + \frac{\mu\gamma_3^{n+1}}{(1+\gamma_3)^{n+1}}\right) \qquad \text{for} \quad L_3 \tag{2.6}$$

and using the Legendre polynomials $\mathcal{P}_n$, we expand the gravitational part of the potential (2.3) as

$$-\frac{1-\mu}{r_1} - \frac{\mu}{r_2} = \sum_{n\geq 2} c_n(\mu)\rho^n \mathcal{P}_n\left(\frac{x}{\rho}\right) ,$$

where $\rho = (x^2+y^2+z^2)^{\frac{1}{2}}$. Introducing the functions

$$T_n(x,y,z) = \rho^n \ \mathcal{P}_n\left(\frac{x}{\rho}\right) ,$$

which are recursively defined through the formulae

$$T_0 = 1\,, \qquad T_1 = x\,, \qquad T_n = \frac{2n-1}{n}xT_{n-1} - \frac{n-1}{n}(x^2+y^2+z^2)T_{n-2} \qquad \forall n \geq 2, \tag{2.7}$$

we obtain that the Hamiltonian (2.4) can be written as

$$\begin{aligned} H(p_x,p_y,p_z,x,y,z,f) = {} & \frac{1}{2}\left(p_x^2+p_y^2+p_z^2\right) + yp_x - xp_y \\ & + \frac{1}{2}\left(1-\frac{r(f)}{h^2}\right)(x^2+y^2+z^2) \\ & - \frac{r(f)}{h^2}\sum_{n\geq 2} c_n(\mu)T_n(x,y,z)\,. \end{aligned} \tag{2.8}$$

2.3. The Hamiltonian in the extended phase space

The Hamiltonian (2.8) is 3D non-autonomous, due to the dependence on time of the true anomaly f. The standard way to make the system autonomous is to *extend* the phase space by considering f as an angle in the Hamiltonian context of action–angle variables and adding a new *dummy* action F, conjugated to f. In the usual units in which $G(m_1+m_2)=1$ with G the gravitational constant and a=1, the time unit is such that the revolution period of the primaries is 2π. Therefore the new angle has unit frequency and, starting from (2.8), we can define the autonomous *null* Hamiltonian $\mathcal{H}$ as

$$\mathcal{H}(p_x,p_y,p_z,F,x,y,z,f) = H + F\,, \tag{2.9}$$

where the dependence on f appears through the radius $r(f)$.

Formally, we can introduce a new time τ which is equal to f; with a little abuse of notation, we denote with a dot the derivative with respect to τ and write the equations of motion as

$$\begin{aligned} \ddot{x} - 2\dot{y} &= \frac{\partial\Omega}{\partial x}, \\ \ddot{y} + 2\dot{x} &= \frac{\partial\Omega}{\partial y}, \\ \ddot{z} + z &= \frac{\partial\Omega}{\partial z}\,, \end{aligned}$$

supplemented by

$$\begin{aligned} \dot{f} &= \frac{\partial\mathcal{H}}{\partial F} = 1, \\ \dot{F} &= -\frac{\partial\mathcal{H}}{\partial f} = \frac{\partial\Omega}{\partial f} = \frac{\mathrm{e}\sin f}{(1+\mathrm{e}\cos f)^2}W(x,y,z)\,, \end{aligned}$$

where W denotes the effective potential

$$W(x,y,z) = \frac{1}{2}(x^2+y^2+z^2) + \frac{1-\mu}{r_1} + \frac{\mu}{r_2} + \frac{1}{2}\mu(1-\mu)\,.$$

The Hamiltonian (2.9) in the extended phase space

$$\mathcal{H}(p_x,p_y,p_z,F,x,y,z,f) = H + F \equiv 0$$

is indeed conserved and is always identically zero. We remark that in the elliptic case there is no equivalent of the Jacobi constant that appears in the circular case (see e.g. [11], Sect.10.3), therefore the conserved quantity (2.9) for the extended system can be usefully exploited as a diagnostic in numerical computations.

2.4. The quadratic part of the Hamiltonian

The general approach to the non-integrable system given by (2.8)–(2.9) is perturbative. Henceforth, we will write $\mathcal{H}$ as a series of the form

$$\mathcal{H}(p_x,p_y,p_z,F,x,y,z,f) = \sum_{n\geq 0}\epsilon^n\mathcal{H}_n\,, \tag{2.10}$$

where ϵ is a *book-keeping* parameter used to arrange terms in this and subsequent series. It is not necessarily related to a physical parameter, but has the role of providing a hierarchy of terms; in practice, after recursions usually implying multiplication of terms, a given series can be reordered and truncated and, in the end, ϵ can be set equal to one. A natural choice is that of considering of order ϵ^n the monomials in p_x,p_y,p_z,x,y,z of degree $n+2$. Moreover, since the dependence on f is provided by the following series expansion

$$\frac{r(f)}{h^2} = \frac{1}{1+\mathrm{e}\cos f} = \sum_{n=0}^{\infty}(-\mathrm{e})^n\cos^n f\,, \tag{2.11}$$

we can replace the expansion (2.11) with the expression

$$\frac{1}{1+\mathrm{e}\cos f} = \sum_{n=0}^{\infty}\epsilon^n(-\mathrm{e})^n\cos^n f\,, \tag{2.12}$$

so that terms proportional to e^n are assumed to be of order ϵ^n.

In order to put the terms of the starting Hamiltonian in a form most suitable for normalization, we need to diagonalize the quadratic part. In view of the expansion (2.12), already the quadratic part in p_x,p_y,p_z,x,y,z of the Hamiltonian contains terms of order greater than zero in the book-keeping. We adopt the simplifying approach of keeping only truly zero-order terms in the quadratic part and therefore we perform the same diagonalizing transformation of the circular case on the quadratic Hamiltonian

$$H_0^{(q)}(p_x,p_y,p_x,x,y,z) = \frac{1}{2}(p_x^2+p_y^2+p_z^2) + yp_x - xp_y - c_2x^2 + \frac{1}{2}c_2y^2 + \frac{1}{2}c_2z^2\,. \tag{2.13}$$

Since the vertical component is already diagonalized, one can limit to define a vector $\xi \equiv (x,y,p_x,p_y)^T$ and write the equations of motion associated to (2.13) as

$$\dot{\xi} = J\nabla H_0^{(q)} = M\xi\,,$$

where the matrices J and M are given by

$$J = \begin{pmatrix} 0 & 0 & 1 & 0 \\ 0 & 0 & 0 & 1 \\ -1 & 0 & 0 & 0 \\ 0 & -1 & 0 & 0 \end{pmatrix}, \qquad M = \begin{pmatrix} 0 & 1 & 1 & 0 \\ -1 & 0 & 0 & 1 \\ 2c_2 & 0 & 0 & 1 \\ 0 & -c_2 & -1 & 0 \end{pmatrix}.$$

Next, after introducing the vector $\tilde{\xi} = (\tilde{x},\tilde{y},\tilde{z},\tilde{p}_x,\tilde{p}_y,\tilde{p}_z)$, one performs a symplectic change of coordinates

$$\tilde{\xi} = C\,\xi \tag{2.14}$$

with C a real matrix (see below for its explicit expression), such that the transformed equations are

$$\frac{d\tilde{\xi}}{dt} = \widetilde{M}\ \tilde{\xi}$$

with

$$\widetilde{M} = \begin{pmatrix} \lambda_x & 0 & 0 & 0 \\ 0 & 0 & 0 & \omega_y \\ 0 & 0 & -\lambda_x & 0 \\ 0 & -\omega_y & 0 & 0 \end{pmatrix}.$$

In complete analogy with the circular case, we introduce the zero-order frequencies

$$\omega_y \equiv \sqrt{-\eta_1}, \quad \omega_z \equiv \sqrt{c_2} \tag{2.15}$$

and the rate

$$\lambda_x \equiv \sqrt{\eta_2}$$

where

$$\eta_1 = \frac{c_2 - 2 - \sqrt{9c_2^2 - 8c_2}}{2}, \qquad \eta_2 = \frac{c_2 - 2 + \sqrt{9c_2^2 - 8c_2}}{2} .$$

The matrix C in (2.14) is defined as

$$C = \left(\frac{a_{+\lambda_x}}{s_1} \quad \frac{a_{\omega_y}}{s_2} \quad \frac{1}{\sqrt{\omega_z}} e_3 \quad \frac{b_{-\lambda_x}}{s_1} \quad \frac{b_{\omega_y}}{s_2} \quad \sqrt{\omega_z} e_6 \right) ,$$

where e_j denote the unit vectors of the canonical basis, the eigenvectors associated to ω_y are $a_{\omega_y} + i b_{\omega_y}$, while those associated to $\pm\lambda_x$ are $a_{+\lambda_x}$, $b_{-\lambda_x}$; finally, the quantities s_1, s_2 are introduced to make the transformation symplectic:

$$s_1 = \sqrt{2\lambda_x((4+3c_2)\lambda_x^2 + 4 + 5c_2 - 6c_2^2)} ,$$
$$s_2 = \sqrt{\omega_y((4+3c_2)\omega_y^2 - 4 - 5c_2 + 6c_2^2)} .$$

As it is well known, since $c_2 > 1$, one obtains that $\eta_1 < 0$, $\eta_2 > 0$, showing that the equilibrium point is of type saddle × center × center and, as a matter of fact, the quadratic part $H_0^{(q)}$ can be written as

$$\tilde{H}_0^{(q)}(\tilde{p}_x, \tilde{p}_y, \tilde{p}_z, \tilde{x}, \tilde{y}, \tilde{z}) = \lambda_x \tilde{x}\tilde{p}_x + \frac{\omega_y}{2}(\tilde{y}^2 + \tilde{p}_y^2) + \frac{\omega_z}{2}(\tilde{z}^2 + \tilde{p}_z^2) .$$

Finally, we introduce complex coordinates through the canonical transformation

$$\tilde{x} = q_1 , \qquad \tilde{p}_x = p_1 ,$$
$$\tilde{y} = \frac{q_2 + i p_2}{\sqrt{2}} , \qquad \tilde{p}_y = \frac{i q_2 + p_2}{\sqrt{2}} ,$$
$$\tilde{z} = \frac{q_3 + i p_3}{\sqrt{2}} , \qquad \tilde{p}_z = \frac{i q_3 + p_3}{\sqrt{2}} .$$

In the eccentric model, such a transformation leads to write the quadratic part of the Hamiltonian as

$$\mathcal{H}_{quadr}(p,q) = \lambda_x q_1 p_1 + i\omega_y q_2 p_2 + i\omega_z q_3 p_3 + F - \sum_{n=1}^{\infty} \epsilon^n (-\mathrm{e})^n \cos^n f \left[\frac{1}{2}(x^2 + y^2 + z^2) + c_2(\mu) T_2(x,y,z) \right] ,$$

where, in the square brackets, x, y, z has to be intended as expressed first in terms of $\tilde{\xi}$ and then in terms of (p,q), while c_2 and T_2 have been defined, respectively, in (2.6) and (2.7). We recognize that the zero-order term in the extended phase space takes the diagonal form

$$\mathcal{H}_0(p,q) = \lambda_x q_1 p_1 + i\omega_y q_2 p_2 + i\omega_z q_3 p_3 + F \tag{2.16}$$

and the starting Hamiltonian series can finally be written as in (2.10)

$$\mathcal{H}(p,q,F,f) = \sum_{k\geq 0} \epsilon^k \mathcal{H}_k(p,q,f) , \tag{2.17}$$

but expressed in the diagonalizing coordinates.

2.5. Center manifold reduction

Perturbation theory is implemented here by constructing a resonant normal form generalizing that obtained in the circular problem [6,7]. It turns out that for typical values of the mass parameter, the two elliptic frequencies ω_y and ω_z in (2.15) are very close to each other [16]; moreover, when extending the notion of frequencies to the elliptic problem, this fact is not substantially changed if the eccentricity is small. Therefore, in order to capture bifurcation phenomena related to the synchronous 1:1 resonance (e.g., *halo* orbits), we proceed to normalize with respect to the *resonant* quadratic part

$$\mathcal{H}_0^{(res)}(p,q) = \lambda_x q_1 p_1 + i\omega_z (q_2 p_2 + q_3 p_3) + F .$$

Namely, we assume that the two elliptic frequencies ω_y and ω_z are equal and we shift their small difference into a first-order term

$$\sum_{n=1}^{\infty} \epsilon^n \mathcal{H}_n = i\epsilon\delta q_2 p_2 + - \sum_{n=1}^{\infty} \epsilon^n (-\mathrm{e})^n \cos^n f \left[\frac{1}{2}(x^2 + y^2 + z^2) + c_2(\mu) T_2(x,y,z) \right] + - \sum_{n=0}^{\infty} \epsilon^n (-\mathrm{e})^n \cos^n f \sum_{j=1}^{\infty} \epsilon^j c_{j+2}(\mu) T_{j+2}(x,y,z) ,$$

by means of the *detuning* parameter δ defined as

$$\delta \equiv \omega_y - \omega_z .$$

In the end, we perform the *center manifold reduction* [3], according to the following result.

Proposition 1. *Consider the Hamiltonian $\mathcal{H}(p,q,F,f)$ in (2.17). There exists a canonical transformation $C : \mathbb{R}^6 \to \mathbb{R}^6$ with $C(p,q) = (P,Q)$, such that $\mathcal{H}$ is transformed to order $N \in \mathbb{N}$ into the 'normal form'*

$$K(P,Q,F) = \lambda_x Q_1 P_1 + i\omega_z (Q_2 P_2 + Q_3 P_3) + i\epsilon\delta Q_2 P_2 + F + \sum_{n=1}^{N} \epsilon^n K_n(Q_1 P_1, P_2, P_3, Q_2, Q_3) + R_{N+1}(P,Q) ,$$

where the polynomials K_n depend on Q_1, P_1 only through their product $Q_1 P_1$, while $R_{N+1}(P,Q)$ is the remainder function of degree $N+1$, which can depend on Q_1, P_1, separately.

We notice that the terms $K_n, n > 0$, satisfy the following properties:

(i) K_n are polynomials of degree $n+2$ in (P,Q);
(ii) the terms K_n satisfy the following *normal form equation:*

$$\{K_n, H_0^{(res)}\}\Big|_{(P,Q)} = 0 \qquad \forall\, n > 0 ,$$

namely they are combinations of monomials in the *kernel* of the linear Hamiltonian operator associated to $H_0^{(res)}$;
(iii) the coefficients of the terms K_n depend on e, but all terms depending on f are eliminated.

Summarizing, the resonant normal form allows us to obtain three relevant results:

1. The normal form depends on the first conjugate pair only through powers of the product $Q_1 P_1$; the hyperbolic dynamics is 'killed' and the center manifold reduction is henceforth obtained by choosing initial conditions such that $Q_1 = 0, P_1 = 0$ (compare with Section 3).

2. We pass from a non-autonomous to an autonomous integrable 3-DOF Hamiltonian system. The dependence on f, which is removed in the normalizing transformation, is maintained in the generating functions which are used to construct approximating solutions for the orbits explicitly depending on the true anomaly of the primaries.

3. The resonant terms allow us to describe bifurcation phenomena associated to the (almost) 1:1 commensurability of the linear frequencies ω_y and ω_z.

3. The resonant normal form

By exploiting a recursion procedure based on the Lie-transform approach [6], according to Proposition 1, we construct the normal form,

$$K(P,Q) = \sum_{n\geq 0}^{N} K_{2n}(P,Q) =$$

$$= \lambda_x Q_1 P_1 + i\omega_z (Q_2 P_2 + Q_3 P_3) + i\delta Q_2 P_2 + \sum_{n=1}^{N} K_{2n}(Q_1 P_1, P_2, P_3, Q_2, Q_3) \ , \tag{3.1}$$

which actually is of order $2N$ since, by symmetry, odd-degree terms do not appear. We have ignored the higher-order remainder and put equal to one the book-keeping parameter. By construction, (3.1) does not depend anymore on f so that F is formally conserved and can be ignored from hereinafter.

At each step of the recursion, we get the generating functions χ_n as

$$\chi_n(P, Q, f), \qquad n = 1, 2, \dots, 2N-1 \ ,$$

where each term is of degree $n+2$ in (P, Q) and possibly trigonometric in $\cos nf$. Following [7], the normal form is expressed in the most compact way by using action–angle variables defined through

$$\begin{aligned}
Q_1 &= \sqrt{J_x} e^{\theta_x} \\
Q_2 &= \sqrt{J_y}(\sin\theta_y - i\cos\theta_y) = -i\sqrt{J_y} e^{i\theta_y} \\
Q_3 &= \sqrt{J_z}(\sin\theta_z - i\cos\theta_z) = -i\sqrt{J_z} e^{i\theta_z} \\
P_1 &= \sqrt{J_x} e^{-\theta_x} \\
P_2 &= \sqrt{J_y}(\cos\theta_y - i\sin\theta_y) = \sqrt{J_y} e^{-i\theta_y} \\
P_3 &= \sqrt{J_z}(\cos\theta_z - i\sin\theta_z) = \sqrt{J_z} e^{-i\theta_z} \ .
\end{aligned}$$

As said above $J_x = Q_1 P_1$ is a formal conserved quantity of the normal form. The motion on the *center manifold* $J_x = 0$ is then described by an effective 2-DOF Hamiltonian of the form

$$K^{(CM)}(J_y, J_z, \theta_y, \theta_z) = \Omega_y J_y + \Omega_z J_z + \sum_{n=1}^{N} K_{2n}(J_y, J_z, \theta_y - \theta_z) \ , \tag{3.2}$$

where the *new* elliptic frequencies can be expanded as powers of the eccentricity up to a given order $0 \le M \le N$:

$$\Omega_y = \sum_{n=0}^{M} \Omega_{y,n} \, \mathrm{e}^n \ , \qquad \Omega_z = \sum_{n=0}^{M} \Omega_{z,n} \, \mathrm{e}^n \tag{3.3}$$

with

$$\Omega_{y,0} = \omega_y, \quad \Omega_{z,0} = \omega_z \ .$$

For further reference, the terms up to third order in the actions are

$$K_2 = \alpha J_y^2 + \beta J_z^2 + J_y J_z(\sigma + 2\tau\cos 2(\theta_y - \theta_z)), \tag{3.4}$$

$$K_4 = \alpha_1 J_y^3 + \beta_1 J_z^3 + \sigma_1 J_y^2 J_z + \sigma_2 J_y J_z^2 + 2(\tau_1 J_y^2 J_z + \tau_2 J_y J_z^2)\cos 2(\theta_y - \theta_z) \tag{3.5}$$

for suitable constant coefficients α, β, σ, τ, α_1, β_1, σ_1, σ_2, τ_1, τ_2. The coefficients of these expansions depend not only on the mass-ratio μ, but also on the eccentricity of the motion of the primaries as terms of the series in e^{2n}. They progressively appear as much as higher is the truncation order of the normal form. For example, truncating at K_4, in K_2 there appear terms proportional to e^2.

The Hamiltonian $K^{(CM)}$ defines an integrable dynamics, since it depends just on the combination angle $\theta_y - \theta_z$: the additional formal integral of motion is

$$\mathcal{E} = J_y + J_z \ .$$

In principle, any initial condition on the center manifold determines a known invariant object, periodic or quasi-periodic. In particular, the nonlinear *normal-modes* $J_y = \text{const}, J_z = 0$ and $J_y = 0, J_z = \text{const}$, respectively produce *planar* and *vertical* Lyapunov orbits. Resonant solutions satisfying $\theta_y - \theta_z = \pm\pi/2$ and suitable values of J_y, J_z, produce the *halo* families. Generic initial conditions produce invariant (Lissajous) tori around each family.

These solutions can be mapped back to the original coordinates by inverting the normalizing transformation. To do this, let us collectively denote the final coordinates corresponding to a given invariant object as $W = (P, Q)$. Then, the original coordinates $w = (p, q)$ approximating the 'actual' object, are given by a series of the form $w = \sum_k \epsilon^k w_k$ with terms given by the sequence

$$\begin{aligned}
w_0 &= W, \\
w_1 &= \{W, \chi_1\}, \\
w_2 &= \{W, \chi_2\} + \frac{1}{2}\{\{W, \chi_1\}, \chi_1\}, \\
&\vdots = \vdots \\
w_k &= \{W, \chi_k\} + \Gamma_k(W, \chi_1, \dots, \chi_{k-1})
\end{aligned} \tag{3.6}$$

for a suitable function Γ_k depending on the generating functions determined at the previous steps. The above formulae allow us to deduce the explicit time-dependence of the solutions. Finally, to plot the solutions in the synodic system, we have to invert the diagonalizing and scaling transformations (see, e.g., [7]). It is worth to observe that either a normal mode or another family of periodic orbits in *generic position* of the normal form [17], in general, *do not* give a periodic orbit in the original coordinates. The dependence on the true anomaly injected in the terms (3.6) by the generating functions χ_k appears at the frequency of the primaries, which is in general not-commensurable with the period of the orbit in the normalizing variables. True periodic orbits can appear as isolated objects only when initial conditions produce such a commensurability. We will provide some examples in Section 5.

4. Halo orbits

The theory of bifurcation of the halo family proceeds in the same way as treated in the circular problem; we refer to [6,7] for more results in the context of the circular problem. Here, we limit the analysis to bifurcations at first-order which, for sake of understanding the relevant mechanism, is perfectly fit.

Hamilton's equations associated to $K^{(CM)}$ in (3.2)-(3.4) are given by

$$\dot{J}_y = 4\tau J_y J_z \sin(2\theta_y - 2\theta_z) \tag{4.1}$$

$$\dot{J}_z = -4\tau J_y J_z \sin(2\theta_y - 2\theta_z) \tag{4.2}$$

$$\dot{\theta}_y = \Omega_y + [2\alpha J_y + \sigma J_z + 2\tau J_z \cos(2\theta_y - 2\theta_z)] \tag{4.3}$$

$$\dot{\theta}_z = \Omega_z + [2\beta J_z + \sigma J_y + 2\tau J_y \cos(2\theta_y - \theta_z)] \ . \tag{4.4}$$

From (4.1)–(4.2) we have that $\dot{J}_y + \dot{J}_z = 0$, so that, in this approximation, $J_y + J_z$ is a constant of motion. According to [6,18], we introduce the following transformation of coordinates

$$\begin{aligned}
\mathcal{E} &= J_y + J_z \\
\mathcal{R} &= J_y \\
\nu &= \theta_z \\
\psi &= \theta_y - \theta_z \ .
\end{aligned} \tag{4.5}$$

The transformed Hamiltonian $K^{(CM)}$, obtained implementing (4.5), reads as

$$K^{(tr)}(\mathcal{E}, \mathcal{R}, F, \nu, \psi) = \Omega_z \mathcal{E} + \delta\mathcal{R} + a\mathcal{R}^2 + b\mathcal{E}^2 + c\mathcal{E}\mathcal{R} + d(\mathcal{R}^2 - \mathcal{E}\mathcal{R})\cos(2\psi) \ , \tag{4.6}$$

where

$$\begin{aligned}
a &= \alpha + \beta - \sigma \ , \\
b &= \beta \\
c &= \sigma - 2\beta \\
d &= -2\tau \ .
\end{aligned}$$

From Hamilton's equations associated to (4.6), we have:

$$\begin{aligned}
\dot{\mathcal{E}} &= 0 \\
\dot{\mathcal{R}} &= 2d\mathcal{R}(\mathcal{R} - \mathcal{E})\sin(2\psi) \\
\dot{\nu} &= \Omega_z + 2b\mathcal{E} + c\mathcal{R} - d\mathcal{R}\cos(2\psi)
\end{aligned}$$

$$\dot{\psi} = \delta + 2a\mathcal{R} + c\mathcal{E} + d(2\mathcal{R} - \mathcal{E})\cos(2\psi) \ .$$

Hence, we recognize that the equilibrium positions $\psi = 0,\ \pi,\ \pm\frac{\pi}{2}$ give $\dot{\mathcal{R}} = 0$; according to [6,18], $\psi = 0, \pi$ are denoted *inclined* orbits and $\psi = \pm\frac{\pi}{2}$ *loop* orbits. The loops are usually dubbed *halo orbits* in the terminology associated to the collinear points. The equilibria, say $\mathcal{R}_{eq}$, are constrained by the condition

$$0 \le \mathcal{R}_{eq} \le \mathcal{E} \ ,$$

so that threshold values of $\mathcal{E}$ will appear determining the bifurcation of the corresponding family. We denote by $\mathcal{E}_N$ a truncation of the series up to an integer order N, say

$$\mathcal{E}_N = \sum_{k=1}^{N} C_k \ \delta^k$$

for suitable real coefficients C_k. Then, we look for a relation on the bifurcating normal mode between $\mathcal{E}$ and E, that is the energy associated with the Hamiltonian (2.8). These equilibrium positions stem from bifurcations from the normal modes when entering the synchronous resonance, since the normal modes lose stability. As said above, normal modes are the periodic orbits along a single axis, which correspond to the solutions of $\mathcal{R} = \mathcal{E}$ for motions along the y-axis and $\mathcal{R} = 0$ for motions along the z-axis. Such normal modes represent, respectively, an approximation of the planar and vertical Lyapunov periodic orbits.

A computation to first order in δ of the energy level E_1 corresponding to a bifurcation to halo orbits is given by

$$E_1 = \Omega_z \mathcal{E}_1 = \Omega_z C_1 \delta \ ,$$

which, going back to the original coefficients, gives the bifurcation value

$$E_1 = \frac{\Omega_z \delta}{\sigma - 2(\alpha + \tau)} \ . \tag{4.7}$$

5. Example: L_1 in the Earth–Moon case

In order to give a workable case, we provide figures for the Earth–Moon case ($\mu = 0.012150586$) with explicit expressions for the equilibrium point L_1, but we remark that the other collinear points can be treated in a similar way Moreover, we make use of our analytical theory, for the parameters of the Earth–Moon system, to find approximate initial conditions for Lyapunov and halo type orbits. Several results are presented here, whereas more cumbersome formulas are provided in Appendix.

5.1. Normal-mode frequencies

We start with the horizontal and vertical frequencies (3.3) of the normal modes computed up to the power 8 in the eccentricity:

$$\begin{aligned} \Omega_y &= 2.33439 + 0.356732\,\mathrm{e}^2 + 0.200957\,\mathrm{e}^4 + 0.139319\,\mathrm{e}^6 + 0.106541\,\mathrm{e}^8 \ , \\ \Omega_z &= 2.26883 + 0.360261\,\mathrm{e}^2 + 0.201856\,\mathrm{e}^4 + 0.139720\,\mathrm{e}^6 + 0.106766\,\mathrm{e}^8 \ . \end{aligned} \tag{5.1}$$

It is worth to observe that these expansions coincide term by term with those obtained in [13] using the Poincaré–Lindstedt method. Fig. 1 shows the graphs of Ω_y and Ω_z for the point L_1 as a function of the eccentricity, when computing a normal form to the order $N = 2$ and as a series expansion in the eccentricity to the order $M = 8$.

5.2. Planar Lyapunov orbits

By inserting the generating functions (A.5)–(A.6) given in the Appendix in the sequence of transformation (3.6), we get the explicit expressions (A.7)–(A.9) for the Cartesian coordinates. Examples of use of these series are provided in this and the following subsections.

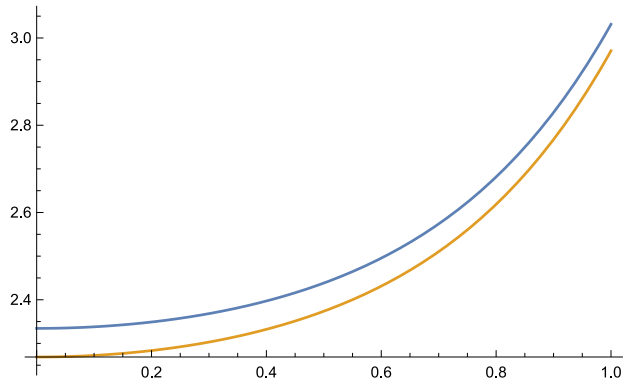

Fig. 1. Ω_y (blue) and Ω_z (yellow) for the point L_1 as a function of the eccentricity in the Earth–Moon system, computed using a normal form to order 2 and a series expansion of the eccentricity to order 8.

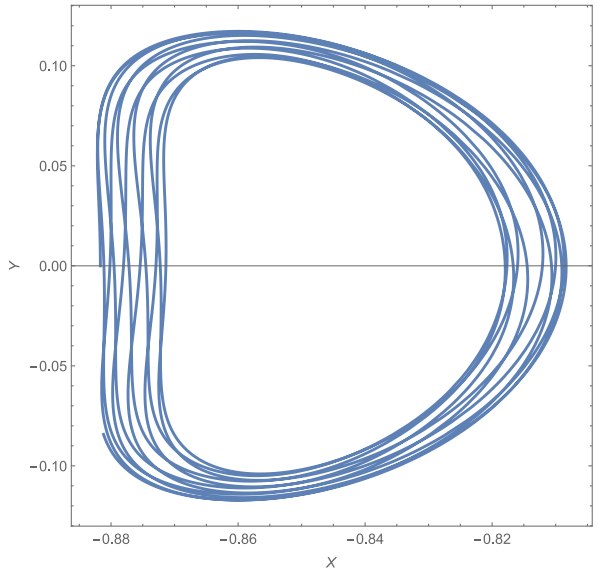

Fig. 2. A planar Lyapunov orbit around L_1 in the Earth–Moon ($\mu = 0.012$) system with $\mathrm{e} = 0.2$. Units are in terms of the Earth–Moon distance.

A normal form solution of the form $J_y = \text{const}, J_z = 0$ produces a planar Lyapunov orbit. Viceversa, a solution $J_y = 0, J_z = \text{const}$ gives a *vertical* orbit. In the final normalizing variables, they correspond to nonlinear oscillations with frequency

$$\kappa_y = \Omega_y + 2\alpha J_y + 3\alpha_1 J_y^2 \tag{5.2}$$

$$\kappa_z = \Omega_z + 2\beta J_z + 3\beta_1 J_z^2 \ . \tag{5.3}$$

As we mentioned before, for planar Lyapunov orbits, then $J_z = 0$. Given κ_y, one determines J_y through (5.2). When mapped back to the original variables, since now the solution explicitly depends on time, we see how a planar Lyapunov orbit around L_1 of the *circular* problem is affected by the elliptic motion of the primaries. As an example, using a big value of the eccentricity in order to magnify its effect ($\mathrm{e} = 0.2$) and taking $J_y = 1$, we get a plot like that presented in Fig. 2.

In the eccentric case, it is possible to find *periodic* Lyapunov orbits, provided that the frequency (5.2) satisfies a condition of the form $\kappa_y = m/n$ with m, n suitable integers. This means that there is a resonance between the orbital period and the synodic period. Once chosen a value for the eccentricity, using expression (5.2), one obtains a value of

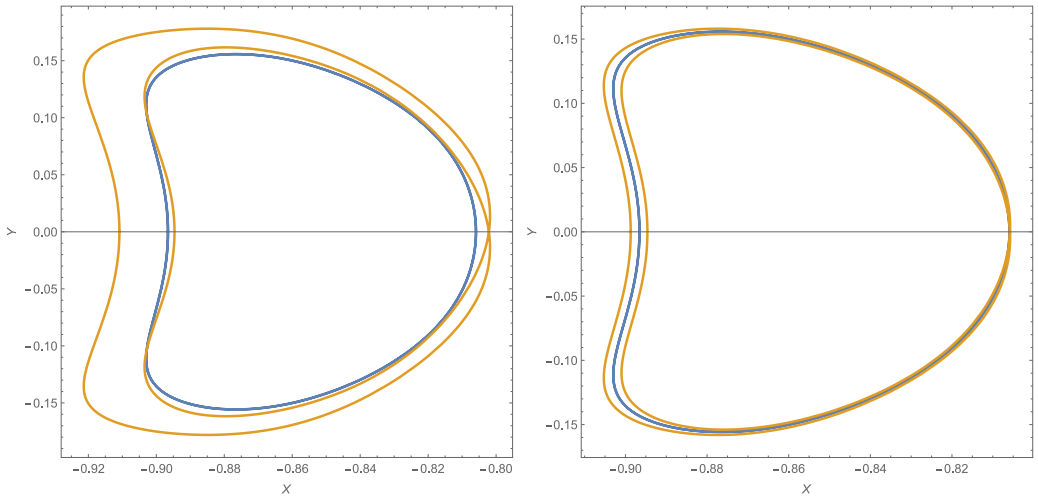

Fig. 3. Periodic planar Lyapunov orbits (in yellow) for $\kappa_y = 2{:}1$ in the Earth–Moon system: on the left we use $e = 0.2$ in order to magnify the effect. On the right the true value $e = 0.0549$ is used. The two orbits are respectively produced by the amplitudes $J_y = 1.075$ and $J_y = 0.9287$. In blue the corresponding orbit in the circular case.

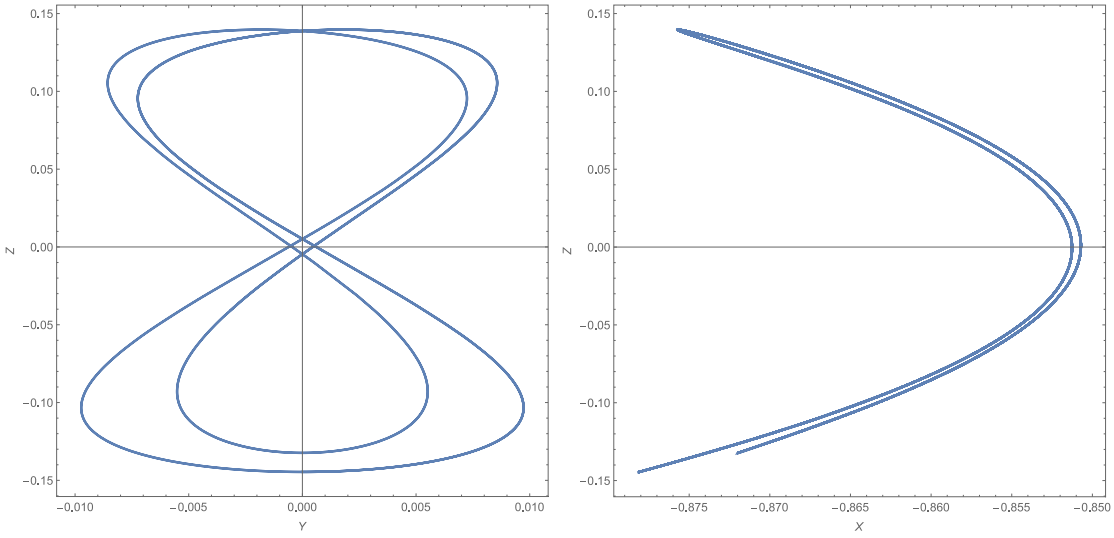

Fig. 4. Periodic vertical Lyapunov orbits for $\kappa_z = 2{:}1$ in the Earth–Moon ($\mu = 0.012$) system but with $e = 0.2$. The amplitude is $J_z = 0.9775$.

the amplitude which produces a certain commensurability. In analogy with the example given in [13], where the approximations have been found with the Lindstedt–Poincaré method, we look for the first-order amplitude producing the resonance condition $\kappa_y = 2{:}1$. By using (5.2) with $e = 0.2$, we find $J_y = 1.075$. In the actual Earth–Moon case ($e = 0.0549$) we find instead $J_y = 0.9287$. By constructing the corresponding solutions in the synodic system, we obtain a fairly good approximation of periodic Lyapunov orbits with the 2:1 ratio, as shown by comparing the right panel of Fig. 3 with Fig. 8.

5.3. Vertical Lyapunov orbits

The procedure to find periodic vertical Lyapunov is the same as that presented in Section 5.2. For vertical Lyapunov orbits, then $J_y = 0$ and equation (5.3) for a given κ_z allows us to determine J_z. Then, Cartesian coordinates X, Y, Z can be found in the Appendix and plotted as a function of the true anomaly f. We notice that, in analogy to the circular case, motion occurs also along X and Y, although the normal form prescribes only an oscillation in the vertical direction.

We report in Fig. 4 an example with $\kappa_z = 2{:}1$, while in Fig. 5 we give an example with $\kappa_z = 3{:}2$.

5.4. Halo orbits

In the case of the Earth–Moon system ($e = 0.0549$), using (A.1)–(A.4), we get that the bifurcation value E_1 (see (4.7)) is given by

$$E_1 = 0.30688 + 0.03221 e^2 \simeq 0.30698 \,,$$

which is slightly bigger than the value 0.306870 found on [6] using a 2nd order resonant perturbation theory.

In order to plot a halo orbit one can again exploit solutions (A.7)–(A.9) of Appendix. This procedure is clearly valid in the framework of a first-order approximation, to keep the algebra as simple as possible.

One starts by choosing a value of $\mathcal{E}$ above the bifurcation value (4.9). Then solves Eq. (4.7) for $\mathcal{R}_{eq}$ and finds:

$$J_{y,H} = \frac{\mathcal{E} + \mathcal{R}_{eq}}{2} \,, \qquad J_{z,H} = \frac{\mathcal{E} - \mathcal{R}_{eq}}{2} \,.$$

After that, one computes the frequency of the orbit:

$$\Omega_H = \left.\frac{\partial \mathcal{K}}{\partial \mathcal{E}}\right|_{\mathcal{R}=\mathcal{R}_{eq}} = \omega_z \frac{2\alpha(1+2\beta\mathcal{E}) + 2\beta(1+\delta) - (\sigma - 2\tau)(2+\delta+(\sigma-2\tau)\mathcal{E})}{2(\alpha+\beta-\sigma+2\tau)}$$

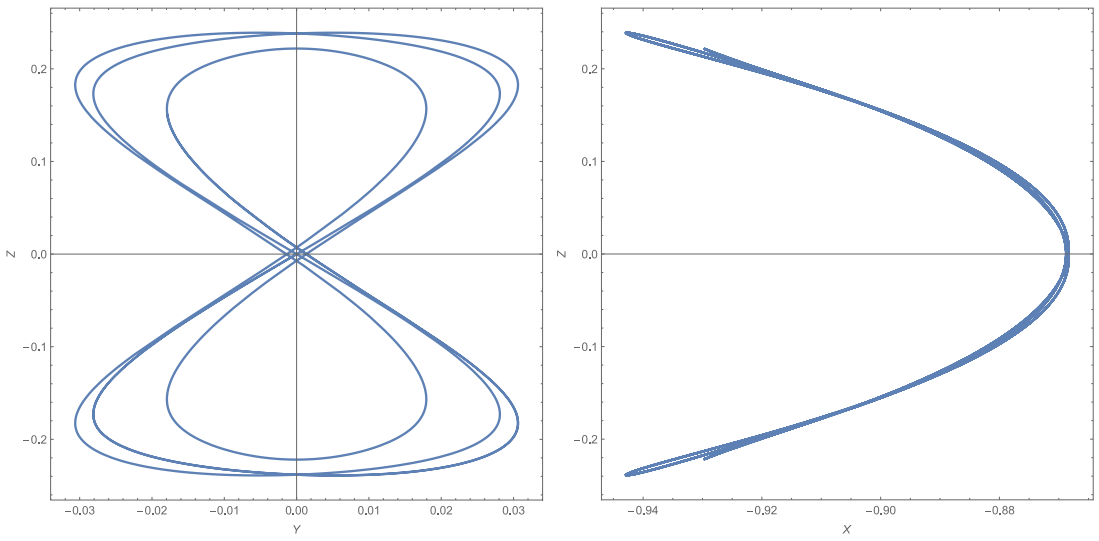

Fig. 5. Periodic vertical Lyapunov orbits for $\kappa_z = 3{:}2$ in the Earth–Moon ($\mu = 0.012$) system but with $e = 0.2$. The amplitude is $J_z = 2.7030$.

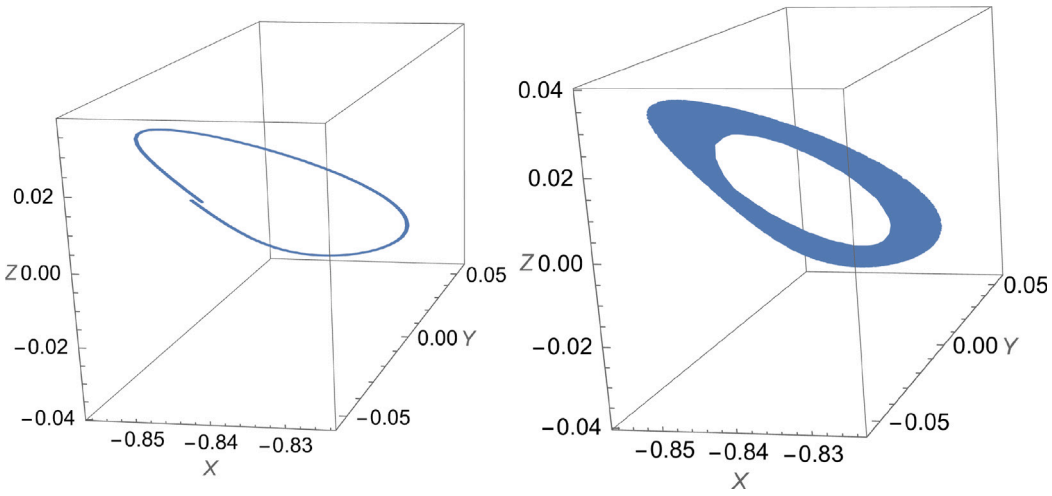

Fig. 6. Halo orbit in the Earth–Moon system ($\mu = 0.012$) around L_1: left, plotted for one-half synodic period; right, plotted for 100 synodic periods.

and obtains

$$\theta_y = \theta_z \pm \pi/2 = \Omega_H f.$$

Plus or minus in the angles give the *northern* and *southern* halo families. Finally, one inserts $J_{y,H}, J_{z,H}, \theta_y, \theta_z$ into (A.7)–(A.9) and plots the orbit.

In Fig. 6 we show an example of a halo-orbit in the Earth–Moon system around L_1, plotted after one-half synodic period and after 100 synodic periods.

6. Validation by numerical simulations

Special care needs to be taken to use the results from the previous sections also in the original rotating–pulsating frame of reference. In this section we highlight two major problems that may arise and also provide a numerical solution to them. We start by taking the approximate initial conditions (AICs), that were obtained from the analytical theory, and use them as initial conditions for a numerical integration of the system (2.2). As an example we provide the orbit shown in Fig. 7 using similar parameters and initial conditions as for the 2:1 resonant planar orbit shown on the right of Fig. 3. In both panels of Fig. 7, we show the orbit in the plane (X, Y) for one synodic period T. From the analytical theory, we expect the orbit to perform two closed loops during the integration time which we do not see on the left. However, taking the time interval $[-T/2, T/2]$ the orbit approaches better the trajectory shown on the right of Fig. 3. Still, we notice that $X'(-T/2)$ does not equal the value $X'(T/2)$ as we should expect for a truly 2:1 resonant periodic planar orbit. We think that the difference can be explained by a combination of factors: (i) the approximation error of the initial conditions obtained from the analytical estimate and (ii) errors in the numerical integration. Moreover, such errors are greatly amplified since the orbit is unstable and the accumulation of the errors over the integration time grows exponentially. As a consequence, we conclude that a direct numerical integration of the AICs using (2.2) is not able to reproduce the correct orbit.

To control the numerical problem (ii), we use the solver NDSolve (Wolfram language, see [19]) using arbitrary precision arithmetic (64

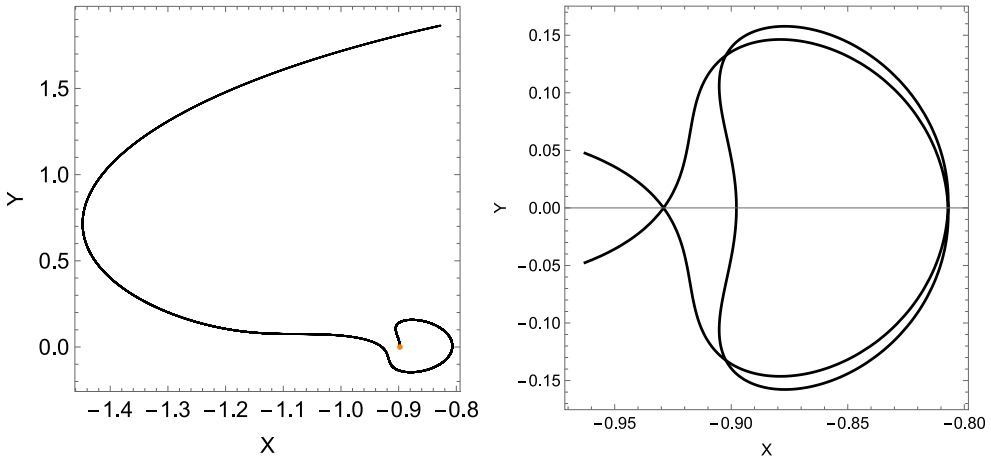

Fig. 7. Same orbit as shown in Fig. 3 for the Earth–Moon system with e=0.0549 based on direct numerical integration of (2.2) with appropriate initial conditions computed using the analytic theory: one complete period $[0, T]$ (left) and $[-T/2, T/2]$ (right) with $T = 2\pi$.

digits in our case). This choice is made to minimize the propagation of the errors due to numerical instabilities when integrating unstable orbits in nonlinear dynamical systems. Several test simulations, together with the analysis of the Jacobian of (2.2) along the solution vector, have been made to guarantee an accuracy of the numerical integration up to 16–20 digits (using for safety a total of 64 digits). Moreover, we checked that the Hamiltonian in the extended phase space is conserved up to machine precision. As a result, we claim to have a reasonable control over the errors stemming from problem (ii).

It remains to tackle the problem (i). As it turns out, even an eighth order normal form does not allow us to obtain a sufficient number of digits in the AIC to overcome problem (i).

However, we propose a solution that implements a numerical refinement of the approximate analytical initial conditions. To this end, let $S = (X, Y, Z, X', Y', Z')$ be the state vector of the orbit and let $S = S(t)$ be the state vector at a given time t. The orbit shown in Fig. 7 is based on the initial condition $S_0^{(0)} = S(t_0 = 0)$ where $S_0^{(0)} = (X_0, Y_0, Z_0, X_0', Y_0', Z_0')$ denotes the AIC from the normal form. Making use of the construction of the AIC, we can deduce the following. Since $S^{(0)}$ has been constructed to obtain a planar 2:1 resonant periodic orbit, we also have the property $S(T) = S(0)$ (called P1) with given period T. Since the periodicity does not depend on the specific choice of f_0 we also have $S(-T/2) = S(T/2)$ (called P2). Looking at the right panel of Fig. 7, we see that property P2 is nearly fulfilled. Let us denote by $\delta S_0^{(0)}$ the initial error of the approximate initial condition labeled $S_0^{(0)}$ and define

$$\delta S_0^{(0)} = S^{(0)}(-T/2) - S^{(0)}(T/2) \,,$$

where we used the upper-script (0) in S to indicate that the solution $S = S(t)$ has been obtained using the initial condition $S_0^{(0)}$. The aim of the numerical refinement method is to find better approximate initial conditions $S_0^{(k+1)}$ such that $|\delta S_0^{(k+1)}| < |\delta S_0^{(k)}|$ with $k = 0, 1, \dots$, where

$$S_0^{(k)} = (X_0^{(k)}, Y_0^{(k)}, Z_0^{(k)}, X_0'^{(k)}, Y_0'^{(k)}, Z_0'^{(k)})$$
$$\delta S_0^{(k)} = S^{(k)}(-T/2) - S^{(k)}(T/2)$$

and where the superscript (k) denotes the kth step of the numerical refinement. Thus, we aim to minimize $|\delta S_0^{(k)}|$ up to $O(\varepsilon)$, say

$$|\delta S_0^{(k)}| < \varepsilon, \tag{6.1}$$

for a given threshold $\varepsilon \in \mathbb{R}_+$. In the case of a planar 2:1 resonant periodic orbit (right panel of Fig. 3), the approximate initial condition has been constructed by making use of the symmetry of the periodic orbit that leads to initial conditions of a specific form:

$$S_0^{(0)} = (X_0^{(0)}, 0, 0, 0, Y_0'^{(0)}, 0) \,.$$

In other words, from the geometry of the planar orbit, 4 out of 6 components vanish exactly:

$$Y_0^{(k)} = Z_0^{(k)} = X_0'^{(k)} = Z_0'^{(k)} = 0 \,, \qquad k \in \mathbb{Z}_+ \,. \tag{6.2}$$

It thus remains to refine $(X_0^{(k)}, Y_0'^{(k)})$. A further reduction of the complexity of the problem can be achieved as follows. In the circular problem the so-called Jacobi constant C_J is a conserved quantity along the orbit. Thus, $C_J = C_J(X_0^{(k)}, Y_0'^{(k)})$ may be used to relate $X_0^{(k)}$ and $Y_0'^{(k)}$ to define $\delta S_0^{(k)}$ to be a scalar function of a single argument x only: $\delta S_0^{(k)} = \delta S_0^{(k)}(x)$ (e.g., $x = X_0^{(k)}$). With this we ensure that we converge to an orbit close to its initial Jacobi constant (and also a related energy level). In the elliptic case, however, $C_J = C_J(t)$ becomes a time dependent quantity. Still, $C_J(0)$ relates $X_0^{(k)}$ with $Y_0'^{(k)}$ at the initial time t_0. We make use of this relation, also in the elliptic problem, to define the error function F_k of a single variable x to be a scalar function:

$$F_k(x) = |\delta S_0^{(k)}(x)| \,. \tag{6.3}$$

Thus, the problem to obtain refined initial conditions that fulfill (6.1) reduces to minimize (6.3) with respect to $x = X_0^{(k)}$.

In practice, we integrate numerically the equations of motion (2.2) using $S_0^{(k)}$, varying $X_0^{(k)}$ until $F_k(X_0^{(k)}) = O(\varepsilon)$, i.e. to meet the requirement provided in (6.1). We therefore notice the presence of an additional parameter in the problem that we need to determine, which is the integration time $T/2$. From the condition for the orbit to be in $2:1$ resonance with the synodic period we conclude $T = 2\pi$. However, as it turns out (6.2) is not necessarily fulfilled at $f = \pm T/2$ for approximate initial conditions $S_0^{(k)}$. A solution to this problem can be found by introducing the integration time itself, let us say $T_{1/2}^{(k)}$, as a free parameter to the problem. At each step of refinement of the initial conditions $S_0^{(k)}$ we determine $T_{1/2}^{(k)}$ by making use of the condition (6.2) itself. In the planar case, we numerically integrate the equations of motion using $S_0^{(k)}$ and determine $T_{1/2}^{(k)}$ from integration time f at which the condition $Y_0^{(k)} = 0$ is fulfilled. We notice that for approximate initial conditions, $X_0'^{(k)}$ does not necessarily vanish when $Y_0^{(k)} = 0$. Defining a second error function

$$G_k(x = X_0^{(k)}) = |X_0'^{(k)}| \quad \text{when} \quad Y_0^{(k)} = 0, \tag{6.4}$$

the correct resonant orbit is therefore determined by the requirement that both conditions, (6.3) and (6.4), vanish together. The implementation of the procedure outlined above requires special care and comes with some solvable technical difficulties: the numerical integrations based on (2.2) need to be very precise, and we need to check the conservation of the Hamiltonian in the extended phase space. In addition, the numerical integrations need to be able to determine very

Table 1
Parameter e and initial conditions X_0, Y_0' (first lines: numerically refined; second lines: analytically approximated), taking $\mu = 0.012150585618$, for planar Lyapunov orbits as shown in Fig. 9. Additional initial conditions are supposed to be zero.

e	X_0	Y_0'
5.49×10^{-5}	−0.895612364839257860	0.380021182345849947
	−0.895653299698303313	0.380142415324720250
5.49×10^{-4}	−0.895630368651718917	0.380013722440848202
	−0.895671692052450123	0.380136116402705453
5.49×10^{-3}	−0.895811058769587885	0.379945336382900154
	−0.895856299492844644	0.380079447631832591
1.10×10^{-2}	−0.896013224440070178	0.379882574878297933
	−0.896062892521110146	0.380029955833534409
2.74×10^{-2}	−0.896628726470471275	0.379777646882579412
	−0.896692190599293081	0.379966565765416729
5.49×10^{-2}	−0.897685606860096430	0.379879928046645625
	−0.897774034521699616	0.380144764189132574

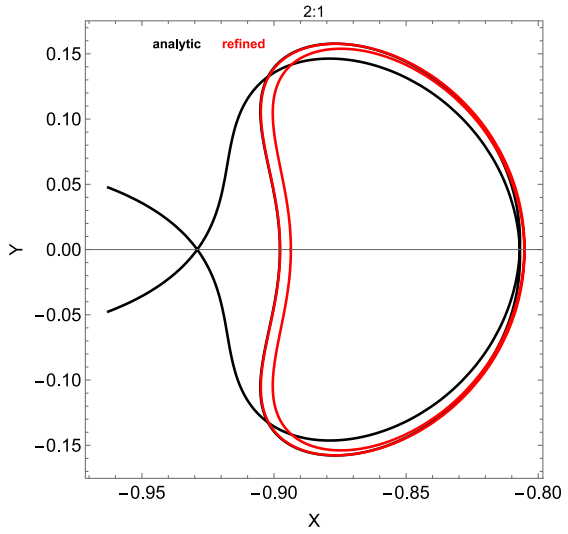

Fig. 8. Same orbit as shown in Fig. 7. The black curve indicates the orbit obtain from approximate analytical initial conditions, the red curve gives the same orbit based on the refined approximate initial conditions (same integration time $T \simeq 2\pi$).

accurately the condition $Y_0^{(k)} = 0$ to calculate $G_k(X_0^{(k)})$. We notice that the convergence of the method does not only depend on the initial choice $S_0^{(k)}$, but also on the choice of the solver to minimize (6.3) and (6.4). In our implementation a combination of a shooting method and Newton's method was used to ensure convergence during the refinement process. We show in Fig. 8 the orbit, mentioned at the beginning of the section, in the (X, Y) plane obtained by implementing the refinement of the analytical initial conditions. The original orbit is shown in black (compare with Fig. 7, right panel), while the numerical refined method is shown in red. For the red orbit ε has been set equal to 10^{-32}. This orbit should be compared with the analytical approximation as shown in Fig. 3, right panel, based on the normal form method, the agreement being very good.

We provide the parameters and initial conditions for several planar Lyapunov orbits in Table 1, where we vary the orbital eccentricity of the Earth–Moon system and fixing the mass parameter. Taking the numerically refined initial conditions (first line in each cell) a numerical integration within the interval $-\pi < f < +\pi$, with $f(0) = 0$, in the synodic reference frame results in the orbits as shown in Fig. 9. The left panel shows the overall structure of the orbits and the right panel a magnification of the region close to the crossing points of the $2:1$ resonant, periodic orbits. Initial conditions have been constructed to provide a maximum error well below machine precision for one full orbital period.

We remark that the method outlined above can be adapted to different kinds of orbits, i.e. resonant and non-resonant orbits, planar and spatial orbits in the circular and elliptic restricted three-body problem. A detailed survey of orbits, based on the present methodology, is planned for a future work.

CRediT authorship contribution statement

Alessandra Celletti: Writing – review & editing, Validation, Supervision, Software, Project administration, Methodology, Investigation, Conceptualization. **Christoph Lhotka:** Writing – review & editing, Visualization, Validation, Software, Methodology, Investigation, Conceptualization. **Giuseppe Pucacco:** Writing – review & editing, Validation, Supervision, Software, Project administration, Methodology, Investigation, Conceptualization.

Declaration of competing interest

The authors declare that they have no known competing financial interests or personal relationships that could have appeared to influence the work reported in this paper.

Data availability

No data was used for the research described in the article.

Acknowledgments

C.L. acknowledges the support from the Excellence Project 2023–2027 MatMod@TOV awarded to the Department of Mathematics, University of Rome Tor Vergata, the project MIUR-PRIN 20178CJAB "New Frontiers of Celestial Mechanics: theory and applications", and the support of GNFM/INdAM.

G.P. acknowledges the support of INFN (Sezione di Roma2) and of GNFM/INdAM.

Appendix

We provide explicit expressions for the normal form, the generating functions and solutions for Lyapunov or halo orbit in terms of time (actually the true anomaly) for the case of the Earth–Moon system. We limit the results to order 4 ($N = 2$). In order to show how the eccentricity of the primaries propagate into the results, we keep it in all formulae. The actual value of the Earth–Moon system is e=0.0549.

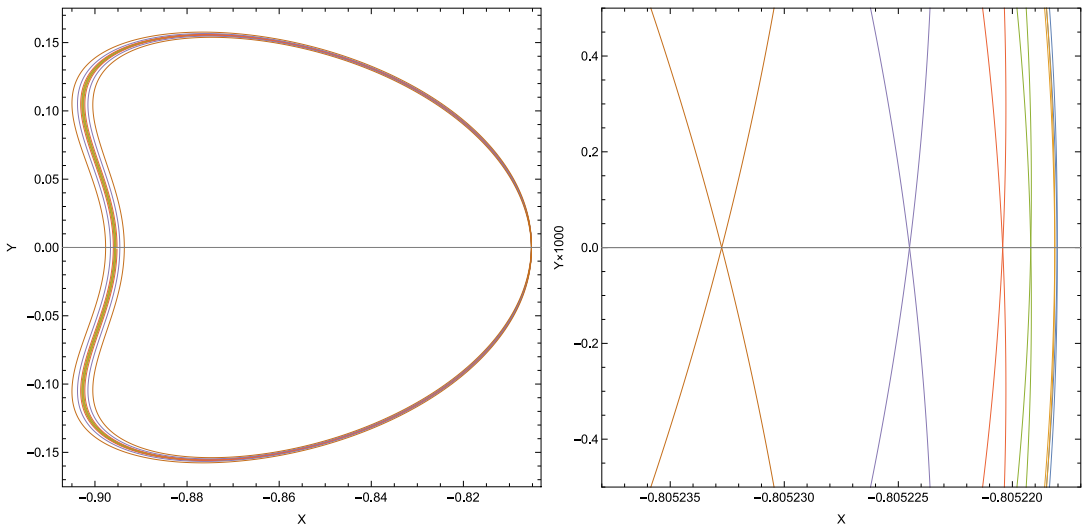

Fig. 9. Planar Lyapunov orbits obtained from numerical integration of the parameters and initial conditions provided in Table 1 (right-to-left of right panel corresponds to top-to-bottom of table values). Integration time $\pm\pi$ with $f(0) = 0$.

The normal form

The terms linear in the actions are recovered by recalling (3.2) and looking at (5.1). For the coefficients appearing in (3.4) and (3.5), we get the following expressions:

$$\alpha = -0.162101380 - 0.005834207\mathrm{e}^2, \tag{A.1}$$
$$\beta = -0.144882524 - 0.006620655\mathrm{e}^2, \tag{A.2}$$
$$\sigma = -0.072614915 - 0.009081915\mathrm{e}^2, \tag{A.3}$$
$$\tau = -0.23307061 - 0.002303888\mathrm{e}^2 \tag{A.4}$$

and

$$\begin{aligned}
\alpha_1 &= -0.01326986,\\
\beta_1 &= -0.008427193,\\
\sigma_1 &= -0.00294965,\\
\sigma_2 &= -0.0023065,\\
\tau_1 &= -0.03174666,\\
\tau_2 &= -0.02757057.
\end{aligned}$$

The generating functions

The first two generating functions (when reduced to the center manifold) are

$$\begin{aligned}
\chi_1 =& 0.12676787 J_y^{3/2}\sin\theta_y + 0.25911415\sqrt{J_y}J_z\sin\theta_y -\\
& 0.052629037 J_y^{3/2}\sin 3\theta_y +\\
& 0.13726658\sqrt{J_y}J_z\sin(\theta_y - 2\theta_z) -\\
& 0.044009618\sqrt{J_y}J_z\sin(\theta_y + 2\theta_z) +\\
& 0.11318452\mathrm{e}J_y\sin(2\theta_y - f) + 0.082529208\mathrm{e}J_z\sin(2\theta_z - f) +\\
& 0.83480871\mathrm{e}J_y\sin f + 0.91403775\mathrm{e}J_z\sin f +\\
& 0.17488611\mathrm{e}J_y\sin(2\theta_y + f) + 0.12918669\mathrm{e}J_z\sin(2\theta_z + f)
\end{aligned} \tag{A.5}$$

and

$$\begin{aligned}
\chi_2 =& -0.086929879\mathrm{e}^2 J_y\sin 2\theta_y + 0.073423235 J_y^2\sin 2\theta_y +\\
& 0.082212129 J_y J_3\sin 2\theta_y - 0.026324747 J_y^2\sin 4\theta_y -\\
& 0.079393462\mathrm{e}^2 J_3\sin 2\theta_z + 0.04150184 J_y J_3\sin 2\theta_z +\\
& 0.051258579 J_3^2\sin 2\theta_z - 0.0096648435 J_3^2\sin 4\theta_z -\\
& 0.033571224 J_y J_3\sin(2\theta_y + 2\theta_z) -\\
& 0.075207468\mathrm{e}^2 J_y\sin(2\theta_y - 2f) -\\
& 0.061131682\mathrm{e}^2 J_3\sin(2\theta_z - 2f) -\\
& 0.012948487\mathrm{e}J_y^{3/2}\sin(\theta_y - f) -\\
& 0.0096070536\mathrm{e}\sqrt{J_y}J_3\sin(\theta_y - f) +\\
& 0.038170957\mathrm{e}J_y^{3/2}\sin(3\theta_y - f) +\\
& 0.11871541\mathrm{e}\sqrt{J_y}J_3\sin(\theta_y - 2\theta_z - f) +\\
& 0.033351938\mathrm{e}\sqrt{J_y}J_3\sin(\theta_y + 2\theta_z - f) -\\
& 0.17836577\mathrm{e}^2 J_y\sin 2f - 0.18013036\mathrm{e}^2 J_3\sin 2f +\\
& 0.085110721\mathrm{e}J_y^{3/2}\sin(\theta_y + f) +\\
& 0.19449047\mathrm{e}\sqrt{J_y}J_3\sin(\theta_y + f) -\\
& 0.035544223\mathrm{e}J_y^{3/2}\sin(3\theta_y + f) -\\
& 0.00060004321\mathrm{e}\sqrt{J_y}J_3\sin(\theta_y - 2\theta_z + f) -\\
& 0.02959452\mathrm{e}\sqrt{J_y}J_3\sin(\theta_y + 2\theta_z + f) +\\
& 0.035853824\mathrm{e}^2 J_y\sin(2\theta_y + 2f) +\\
& 0.015525144\mathrm{e}^2 J_3\sin(2\theta_z + 2f)\ .
\end{aligned} \tag{A.6}$$

Note that all terms explicitly depending on the true anomaly f vanish when e=0.

Orbits

Here we report the analytic solutions in Cartesian coordinates in the synodic frame for orbits in the Earth–Moon case with, as above, arbitrary eccentricity of the primaries. These expressions can be used to plot approximate orbits, when the frequencies are computed as in

(5.2)-(5.3) and substituted into

$$\theta_y = \kappa_y(J_y, J_z)f, \quad \theta_z = \kappa_z(J_y, J_z)f,$$

once given values of the actions J_y, J_z are chosen. As discussed above in Section 5.2 this is particularly useful when looking for approximations of periodic orbits. In the analytical plots of Section 5 we made the further simplifying assumption of approximating f with the mean anomaly $\ell = nt$. The Cartesian coordinates X, Y, Z are given by the following expressions:

$$\begin{aligned}
X(f) = &-0.83691513 - 0.028066789J_y - 0.028684328J_z - \\
&0.042530591\sqrt{J_y}\cos\theta_y + 0.011616838e^2\sqrt{J_y}\cos\theta_y - \\
&0.0072538664J_y^{3/2}\cos\theta_y - 0.0080462385\sqrt{J_y}J_z\cos\theta_y + \\
&0.011473421J_y\cos 2\theta_y + 0.0030761579J_y^{3/2}\cos 3\theta_y + \\
&0.0012147932\sqrt{J_y}J_z\cos(\theta_y - 2\theta_z) + 0.012054911J_z\cos 2\theta_z + \\
&0.002869961\sqrt{J_y}J_z\cos(\theta_y + 2\theta_z) - \\
&0.0004757866e^2\sqrt{J_y}\cos(\theta_y - 2f) + \\
&0.0038943343e\sqrt{J_y}\cos(\theta_y - f) - 0.0082945643eJ2\cos(2\theta_y - f) - \\
&0.009169466eJ_z\cos(2\theta_z - f) - 0.0083767837eJ_y\cos f - \\
&0.010112763eJ_z\cos f - \\
&0.037106626e\sqrt{J_y}\cos(\theta_y + f) + 0.013195973eJ_y\cos(2\theta_y + f) + \\
&0.015384742eJ_z\cos(2\theta_z + f) - 0.0082310824e^2\sqrt{J_y}\cos(\theta_y + 2f)\,,
\end{aligned} \tag{A.7}$$

$$\begin{aligned}
Y(f) = &0.15253593\sqrt{J_y}\sin\theta_y - 0.038529801e^2\sqrt{J_y}\sin\theta_y + \\
&0.011312977J_y^{3/2}\sin\theta_y + 0.0030420108\sqrt{J_y}J_z\sin\theta_y + \\
&0.011580803J_y\cos\theta_y\sin\theta_y + 0.0040746736J_y^{3/2}\sin 3\theta_y - \\
&0.0079110266\sqrt{J_y}J_z\sin(\theta_y - 2\theta_z) - \\
&0.01330702J_z\cos\theta_z\sin\theta_z + \\
&0.001691008\sqrt{J_y}J_z\sin(\theta_y + 2\theta_z) + \\
&0.018042238e^2\sqrt{J_y}\sin(\theta_y - 2f) - \\
&0.049106567e\sqrt{J_y}\sin(\theta_y - f) - \\
&0.0039015441eJ_y\sin(2\theta_y - f) + \\
&0.004349965eJ_z\sin(2\theta_z - f) + 0.0079996739eJ_y\sin f + \\
&0.0064257087eJ_z\sin f + 0.091803411e\sqrt{J_y}\sin(\theta_y + f) + \\
&0.010214749eJ_y\sin(2\theta_y + f) - \\
&0.011359961eJ_z\sin(2\theta_z + f) + \\
&0.006618954e^2\sqrt{J_y}\sin(\theta_y + 2f)\,,
\end{aligned} \tag{A.8}$$

$$\begin{aligned}
Z(f) = &-0.037811696\sqrt{J_y}\sqrt{J_z}\sin(\theta_y - \theta_z) - \\
&0.005705595J_y\sqrt{J_z}\sin(2\theta_y - \theta_z) - \\
&0.14171043\sqrt{J_z}\sin\theta_z + 0.039184292e^2\sqrt{J_z}\sin\theta_z - \\
&0.0013614348J_y\sqrt{J_z}\sin\theta_z - 0.0068725065J_z^{3/2}\sin\theta_z - \\
&0.0027392183J_z^{3/2}\sin(3\theta_z) - \\
&0.012122967\sqrt{J_y}\sqrt{J_z}\sin(\theta_y + \theta_z) - \\
&0.0051006101J_y\sqrt{J_z}\sin(2\theta_y + \theta_z) - \\
&0.019654877e^2\sqrt{J_z}\sin(\theta_z - 2f) - \\
&0.019284097e\sqrt{J_y}\sqrt{J_z}\sin(\theta_y - \theta_z - f) + \\
&0.053069093e\sqrt{J_z}\sin(\theta_z - f) + \\
&0.0081153711e\sqrt{J_y}\sqrt{J_z}\sin(\theta_y + \theta_z - f) - \\
&0.018253022e\sqrt{J_y}\sqrt{J_z}\sin(\theta_y - \theta_z + f) - \\
&0.083071445e\sqrt{J_z}\sin(\theta_z + f) - \\
&0.020585513e\sqrt{J_y}\sqrt{J_z}\sin(\theta_y + \theta_z + f) - \\
&0.0049915983e^2\sqrt{J_z}\sin(\theta_z + 2f)\,.
\end{aligned} \tag{A.9}$$

References

[1] C.C. Conley, Low energy transit orbits in the restricted three-body problem, SIAM J. Appl. Math. 16 (1968) 732–746.
[2] W.S. Koon, W.L. Lo, J.E. Marsden, S.D. Ross, Dynamical Systems, the Three-Body Problem and Space Mission Design, 2011, Mission Design Book Online.
[3] À. Jorba, J. Masdemont, Dynamics in the center manifold of the collinear points of the restricted three body problem, Phys. D 132 (1999) 189–213.
[4] D.L. Richardson, Analytic construction of periodic orbits about the collinear points, Celest. Mech. 22 (1980) 241–253.
[5] G. Gómez, J.M. Mondelo, The dynamics around the collinear equilibrium points of the RTBP, Phys. D 157 (2001) 283–321.
[6] A. Celletti, G. Pucacco, D. Stella, Lissajous and Halo orbits in the restricted three-body problem, J. Nonlinear Sci. 25 (2) (2015) 343–370.
[7] M. Ceccaroni, A. Celletti, G. Pucacco, Halo orbits around the collinear points of the restricted three-body problem, Phys. D 317 (2016) 28–42.
[8] S. Bucciarelli, M. Ceccaroni, A. Celletti, G. Pucacco, Qualitative and analytical results of the bifurcation thresholds to halo orbits, Ann. Mat. Pura Appl. (4) 195 (2016) 489–512.
[9] T. Luo, M. Xu, Y. Dong, Natural formation flying on quasi-halo orbits in the photogravitational circular restricted three-body problem, Acta Astronaut. 149 (2018) 35–46.
[10] R. Broucke, Stability of periodic orbits in the elliptic, restricted three-body problem, AIAA J. 7 (6) (1969) 1003–1009.
[11] V. Szebehely, Theory of Orbits, Academic Press, New York and London, 1967.
[12] A. Celletti, Stability and Chaos in Celestial Mechanics, Springer-Verlag, Berlin; published in association with Praxis Publishing Ltd. Chichester, 2010.
[13] X.Y. Hou, L. Liu, On motions around the collinear libration points in the elliptic restricted three-body problem, Mon. Not. R. Astron. Soc. 415 (2011) 3552–3560.
[14] H. Peng, X. Shijie, Stability of two groups of multi-revolution elliptic halo orbits in the elliptic restricted three-body problem, Celest. Mech. Dyn. Astron. 123 (2015) 279–303.
[15] F. Ferrari, M. Lavagna, Periodic motion around libration points in the elliptic restricted three-body problem, Nonlinear Dyn. 93 (2018) 453–462.
[16] G. Pucacco, Structure of the centre manifold of the L_1, L_2 collinear libration points in the restricted three-body problem, Celest. Mech. Dyn. Astron. 131 (2019) 44.
[17] J.A. Sanders, F. Verhulst, J. Murdock, Averaging Methods in Nonlinear Dynamical Systems, Springer-Verlag, Berlin Heidelberg, 2007.
[18] G. Pucacco, A. Marchesiello, An energy–momentum map for the time-reversal symmetric 1:1 resonance with $\mathcal{Z}_2 \times \mathcal{Z}_2$ symmetry, Phys. D 271 (2014) 10–18.
[19] Wolfram Mathematica (Version 13.2), Wolfram Research (2024) https://reference.wolfram.com/language/ref/NDSolve.html.